



Determination of groundwater potential by using geoelectrical method and petrographic analysis in Rawalakot and adjacent areas of Azad Kashmir, sub-Himalayas, Pakistan

Abrar Niaz¹ · Muhammad Rustam Khan¹ · Umer Ijaz¹ · Muhammad Yasin¹ · Fahad Hameed¹

Received: 2 May 2017 / Accepted: 9 August 2018 / Published online: 23 August 2018
© Saudi Society for Geosciences 2018

Abstract

The current study is carried out for the determination of groundwater potential in District Rawalakot Azad Jammu and Kashmir (AJ&K) Pakistan by using electrical resistivity method and petrographic analysis of the area. The tape-compass-clinometers method was used in section measurement to understand the facies and depositional environment. The electrical resistivity survey was carried out in the project area in sub-Himalayan Siwaliks system of Pakistan to overcome water scarcity in a few regions. The area was chartered with the Schlumberger configuration up to the AB/2 depth of 150 m. The ABEM Terrameter SAS 4000 (Sweden) and accessories were used to acquire vertical electrical soundings in 24 locations. The results obtained through the 2D and 3D isoresistivity maps of apparent resistivity for 15, 45, and 130 m spacings, the 3D isoresistivity maps of transverse resistance and anisotropy, the VES curve types, and the measured stratigraphic section of surface rocks revealed the confined or semi-confined type aquifers within sedimentary formations. The petrographic analysis indicates the clues of the secondary porosity and fluid migrations through the rocks.

Keywords Vertical electrical sounding (VES) · Petrography · Depositional environment · Schlumberger configuration · Sub-Himalayan Siwaliks

Introduction

Groundwater forms the largest, easily accessible and an important natural resource of water. The intricate joints, fractures, and tiny pore spaces of rocks together hold immense volume of groundwater (Lutgens et al. 2014). The groundwater free from bacteriological pollution and hence safe for household utilization constitutes half of all the drinking water worldwide (Elizondo and Lofthouse 2010; Siebert et al. 2010; Smith et al. 2016; Okafor and Mamah 2012). The annual rate of worldwide groundwater extraction is about 982 km³ where 70% portion is utilized in agriculture sector (Margat and Van der Gun 2013). With the growth of population at an enormous rate, the groundwater extraction is expected to increase from 15,000 m³/day at present to 37,000 m³/day by 2025 (Maury

and Balaji 2014). Hence, the demand of water can be overcome by the identification of potential aquifers during the demarcation of subsurface geology.

There are several methods worked out in practice for the assessment of hydrogeological conditions, and among these, the geoelectrical resistivity methods are well known for effectiveness, reliability, and feasibility (Martinelli 1978; Oseji et al. 2006; Khalil 2010; Sikandar et al. 2010; Joshua et al. 2011). These methods have been widely employed for the subsurface mapping, groundwater assessment, exploration, and salinity demarcation relying on resistivity variations (Barseem et al. 2013; Choudhury et al. 2001; Khaled and Galal 2012). The integration of various subsurface parameters taken out from resistivity measurements can be effective as electrical resistivity properties correlated with hydraulic properties based on the grain size distribution, fabric, structure, and heterogeneities (DeLima et al. 2005; Hubbard and Rubin 2005; Niwas et al. 2006). The vertical electrical sounding (VES) is one of the most versatile methods used in groundwater resource estimation and exploration (Balaji et al. 2010; Khalil 2010).

The study area district Rawalakot Azad Jammu and Kashmir is located at 250 km from Islamabad Pakistan, in

✉ Abrar Niaz
abrar.niaz@ajku.edu.pk

¹ Institute of Geology, University of Azad Jammu and Kashmir, P.O. Box 13100, Muzaffarabad, Azad Jammu and Kashmir, Pakistan

the sub-Himalayas, a part of Hazara Kashmir syntaxes (Thakur et al. 2010). The area lies between longitudes $73^{\circ}37'45''$ to $73^{\circ}49'01''$ east and latitudes $33^{\circ}47'52''$ to $33^{\circ}51'51''$ north covering parts of Survey of Pakistan toposheet no. 43 G/9 (Fig. 1). The topography of the area is extremely rugged with steep hills and valleys having a diverse landscape with an elevation between 500 to 2256 m from the sea level. The study area (Fig. 1) possesses thick Neogene sedimentary rocks. These rocks include the lithologic assemblages of planar bedded sandstone, shale, claystone of Nagri Formation (Fig. 2) and conglomerates passim in the Murree, Nagri, Dhok Pathan formations and recent alluvium. A measured stratigraphic section of surface sediments is shown in Fig. 2. The base of the formation includes mudstone/claystone alternating with shale and sandstone (Fig. 2). The mudstone ranges in thickness from 8.0 to 23.5 m. The shale beds have average thickness of about 53.6 to 63 m and yield leaf imprints and carbonate concretions. The sandstone of the section varies in thickness from 20.5 to 58.5 m thickness. The wood fossils and exotic conglomerate clasts are tessellated in few beds (Fig. 2). The conglomerate clasts have owned few millimeters to several centimeters diameter with rounded to sub-rounded and disc-shaped outlines. Moreover, the fluvial structures

formed by floundering flow velocities include planar bedding and ripple laminations (Fig. 2).

The sandstone is interbedded with shale (Fig. 2) and acts as confined aquifers in a few areas. The rocks of the region are faulted (Fig. 1) and fractured. The spurt of water through fractures and some spouting through poorly consolidated sediments has been noticed. In addition, the area is drained by few intermittent streams, inundated during summer monsoon rainy season. The average rainfall in the area is 476 mm due to monsoon in July and August (Climate-data.org). The streams of the area in some places have been harnessed to form small dams. The stored water in these small dams is consumed during the extremely parched summer. However, most of the population is facing water shortage. So, the water scarcity is a major problem in few regions.

Previously, the area has not been investigated for groundwater exploration. Only a few springs and piped water supply are the reliable but insufficient source of fresh water for inhabitants. An attempt has been made to estimate groundwater potential and depth beside the thickness of subsurface layers and their water-yielding capabilities using the VES and petrographic analysis.

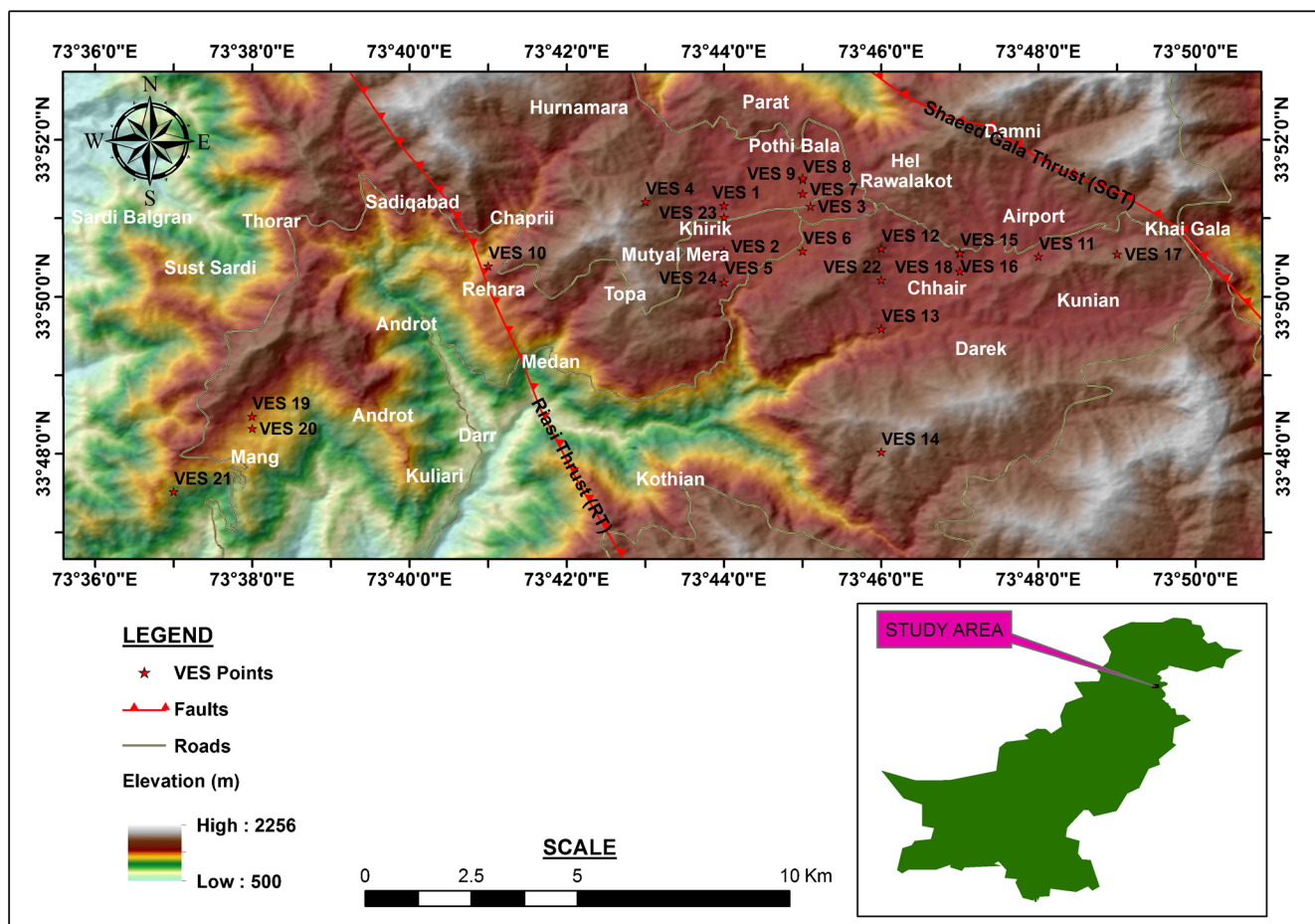


Fig. 1 Showing the location of study area, VES points, and regional faults on digital elevation model (DEM)

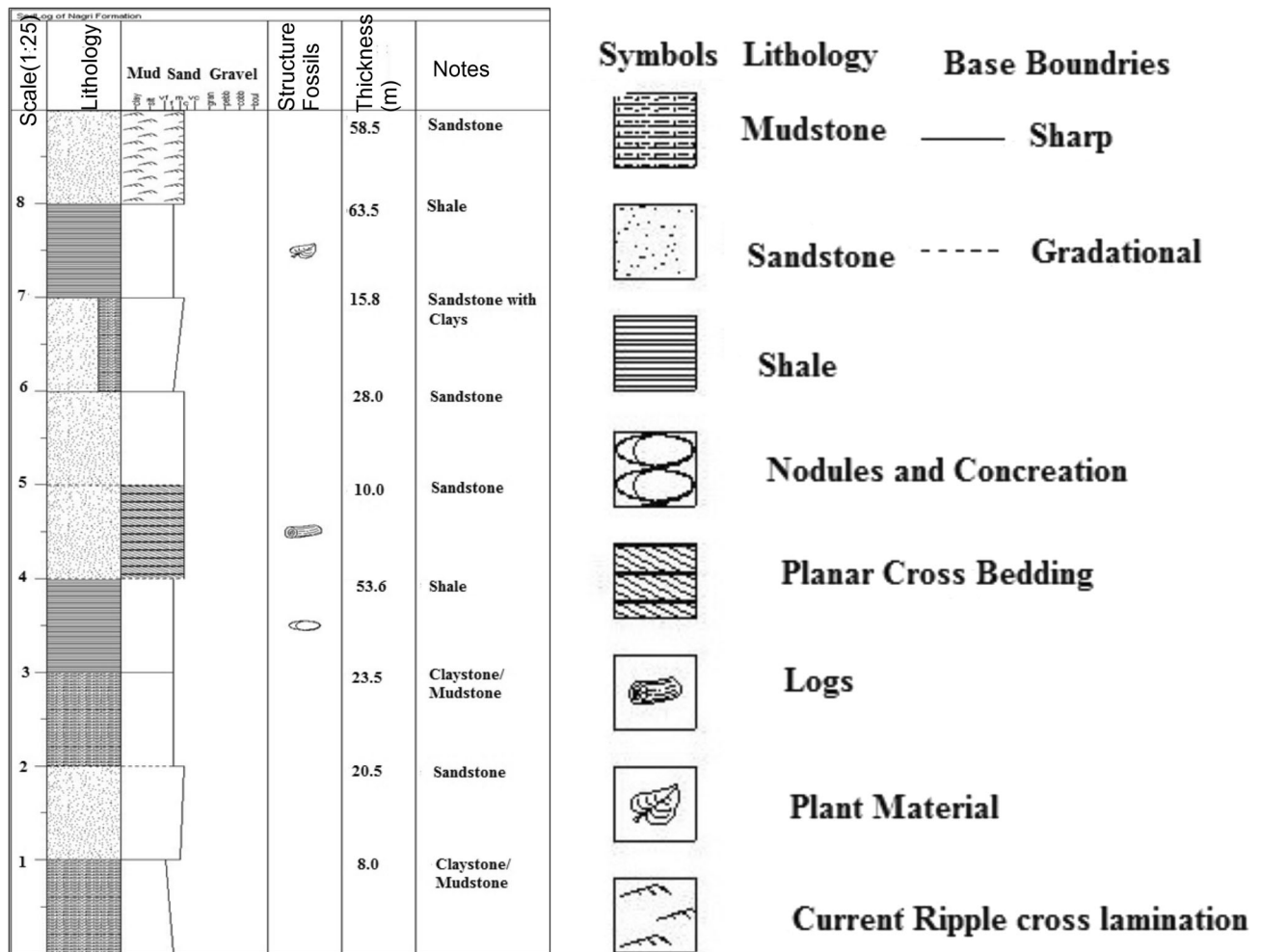


Fig. 2 A typical stratigraphic section exposed at Medan area

Materials and methods

The electrical resistivity method was embarked in the study area in accordance with the previously applied methods for the exploration of water resources (Dobrin 1988; Ozcep et al. 2009; Alile et al. 2011). In other words, a resistivity survey was accomplished in the near surface sediments and in milder climatic conditions to access the information regarding the presence of water in the rocks. The area was chartered with the Schlumberger configuration in lieu of other methods. For this purpose, vertical electrical soundings (VES) were used in 24 locations up to the total AB/2 depth of 150 m. The precise locations of these stations were positioned on the digital elevation model (DEM) using global positioning system (GPS). The paraphernalia used for VES includes ABEM Terrameter SAS 4000 (Sweden) and accessories. A symmetric increase in the spread distance of the deployed current and potential electrodes was paced out for deeper penetrations. Three and four layers of curve’s shapes were obtained in qualitative

interpretations (Table 1). In addition, the IPI2win software has formulated the resistivity model of earth (Orellana and Mooney 1966). The thicknesses and true resistivities of the subsurface layers have been calculated and enumerated under Table 2. Furthermore, the computer software (Surfer V.10) was assiduously used to portray the iso-resistivity maps. The low (depression mark) and high values (peak) have been illustrated on the 2D and 3D iso-resistivity maps of apparent resistivity. Moreover, the thickness of rocks was gauged during field work from the well-exposed sections of Nagri Formation (Middle, Siwaliks) in the area, using Tape-compass Clinometer method (Compton 1985) in order to understand facies and depositional environment of rocks. However, the thickness, lithology, fossils, and sedimentary structures (Fig. 2) were plotted on the software Sed. Log 3.0 version. The thin sections of rock samples were prepared at Geoscience advance research laboratory, Islamabad, Pakistan to understand mineralogy of rocks. However, besides mineralogy, the deformation in mineral grains and

yielding to secondary porosity was encountered during petrographic study. The area has been deformed by regional faults in the region known as Shaeed Gala Thrust and Riasi Thrust (Rustam et al. 2016) as shown on DEM.

Results

Apparent resistivity

The apparent resistivity maps have been made at different electrode spacing to delineate the resistivity variation with depth.

2D iso-resistivity map at 15 m spacing

The apparent resistivity for 15 m spacing falls between 13.16 and 68.99 Ωm on the corresponding iso-resistivity map displayed in Fig. 3. The analysis reveals highest apparent resistivity values of 68.99, 66.671, 44.455, and 41.623 Ωm at VES 24, VES 15, VES 18, and VES1, respectively. On the other hand, the lowest apparent resistivity values of 13.16, 13.498, 18.511, 21.938, and 23.33 Ωm have been interpreted at VES 20, VES 3, VES 6, VES13, and VES9, respectively.

Table 1 The interpreted curve types of the study area

VES No.	Curve types	No. of layers
1	A	3
2	A	3
3	H	4
4	H	4
5	H	4
6	K	2
7	K	3
8	K	3
9	A	3
10	A	3
11	HA	4
12	H	4
13	K	4
14	K	2
15	A	3
16	KA	4
17	A	3
18	HK	4
19	K	3
20	K	3
21	A	3
22	A	3
23	H	4
24	HK	4

The 3D map (Fig. 4) displaying peak at the northern portion of the project area has figured out the presence of sandstone as compared to the presence of clays and boulder clays in the remaining areas. The depression is also visible in this region. Furthermore, the southwestern portion also portrays low values corresponding to VES19, VES20, and VES 21.

2D iso-resistivity map of apparent resistivity at 45 m spacing

The apparent resistivity for 45 m spacing has values lying between 4.57 and 86.585 Ωm on the corresponding iso-resistivity map (Fig. 5). The highest apparent resistivity values of 86.585, 84.675, 69.305, and 64.281 Ωm have been detected at VES 19, VES 10, VES12, and VES4, respectively. The lowest apparent resistivity values of 4.57, 14, 15.716, and 20.623 Ωm have been numerically calculated at VES 3, VES 6, VES13, and VES 8 respectively.

2D iso-resistivity map of apparent resistivity at 130 m spacing

The apparent resistivity for 130 m spacing falls at 8.93 to 100.1 Ωm on the corresponding iso-resistivity map (Fig. 6). The highest values of 100.1, 94.228, 76.258, and 73.493 Ωm have been numerated at VES 4, VES11, VES22, and VES 12, respectively, contrary to the lowest apparent resistivity values of 8.93, 12.67, 21.874, and 25.71 Ωm at VES 3, VES13, VES 8, and VES 7, respectively.

The 3D map (Fig. 7) displaying three low peaks at the north and north eastern portion of the study area has figured out clays with maximum apparent resistivity of almost 100.1 Ωm . However, the rest of the area depicts low resistivity values.

3D iso-resistivity map of transverse resistance

The properties of the conducting layers are determined in terms of longitudinal conductance and those of the resistive layer by transverse resistance (Yungul 1996). This is the total resistance through a 1-m column cut perpendicular to the plane (Parasnis 1979; Nwanko et al. 2011). The decrease in resistivity pointing towards groundwater potential in the area (Gowd 2004; Joseph 2012; Niaz et al. 2016).

The 3D map (Fig. 8) displaying three peaks has figured out the highest transverse resistance values at VES 5, VES12, and VES 19 in central portion of study area. The rest of the areas have revealed lowest resistivity values with good groundwater potential.

Table 2 The interpreted subsurface geology based on geoelectric data

VES No.	Thickness of each layer (h) m	True resistivity (St) (Ohm m)	Depth (meters)	Lithology
1	3.07	21.5	3.07	Clays
	86.3	25.2	89.1	Mudstone
		311		Sandstone
2	0.574	25.2	0.574	Clays
	0.975	58.2	1.55	Mudstone
	10.9	17.2	12.5	Clays
		2397		Sandstone
3	1.98	39.8	1.98	Surface materials
	8.51	9.66	10.5	Boulder clays
	42.3	2.13	52.8	Clays
		594		Sandstone
4	1	2.21	1	Clays
	1.87	0.841	2.87	Boulder clays
		1161		Sandstone
5	1	100	1	Clays
	60.2	59.9	61.2	Sandy clays
		10.6		Clays
6	1	90.3	3.33	Clays
	2.07	99.8		Sandy clays
		22.8		Clays
		23.4	1	Clays
7	13.4	26.1	14.1	Mudstone
		18.6		Clays
	1.61	34.8	1.61	Clays
	2.96	49.3	4.58	Clayey sand
8		20.4		Clays
	2.9	69.7	2.9	Clays
	80.7	23.2	83.6	Mudstone
		3641		Sandstone
9	25.4	22.1	25.4	Clays
	49.4	38.4	74.8	Sandy clays
		88.5		Clays
10	1.05	53.3	1.05	Clays
	3.34	16.1	4.39	Boulder clays
	28.5	42.4	32.92	Siltstone
		449		Sandstone
11	7.14	19.6	7.14	Clays
	11.9	291	19.1	Sandstone
		43.1		Clays
12	30.1	38.4	3.01	Clays
	78.6	15.4	81.6	Sandy clays
		3.43		Clays
13	1	1.38	1	Clays
	2.01	1.13	3.01	Siltstone
		369		Sandstone
14	18.3	45.6	4.28	Clays

Table 2 (continued)

VES No.	Thickness of each layer (h) m	True resistivity (St) (Ohm m)	Depth (meters)	Lithology
15	87.9	24.9		Mudstone
		0.101	8.79	Clays
		32.7	1	Clays
16	1	84.9	3.18	Boulder clays
	2.18	15.1	10.1	Clays
	6.92	69.1		Sandstone
		28.1	7.16	Clays
17	1.04	20.9	14.3	Mudstone
	3.61	45.8	88.2	Clays
		40.9	1	Surface material
18	2.62	61.7	3.62	Mudstone
	9.51	32.6	13.1	Clays
		66.3		Boulder clays
	9.41	19.9	9.41	Clays
19	19.4	302	28.8	Sandstone
		0.639		Clays
	0.574	25.2	0.574	Clays
	0.975	58.2	1.55	Clayey sand
20	10.9	17.2	12.5	Clays
		2397		Sandstone
	1	71.2	1	Clays
	22.7	32.5	23.7	Boulder clays
21		57.7		Clays
	3.47	60.6	3.47	Clays
	10.7	25.8	14.2	Mudstone
		92.6		Clays
22	2.94	37.1	2.94	Clays
	22.5	26.6	25.4	Mudstone
		32.6		Clays
	1	77.6	1	Clays
23	8.04	53.1	9.04	Mudstone
	18.1	123	27.2	Sandstone
		56.6		Clays

Anisotropy

When resistivity of the rock varies with direction of current flow, the rock is said to be anisotropic. A co-efficient of anisotropy is found by taking the square root of the ratio of resistivities (Olasehinde and Bayewu 2011) measured in two principle directions, mathematically:

$$\lambda = (\rho_t / \rho_l)^{1/2} \tag{1}$$

where

λ coefficient of anisotropy

$\rho_t = T$

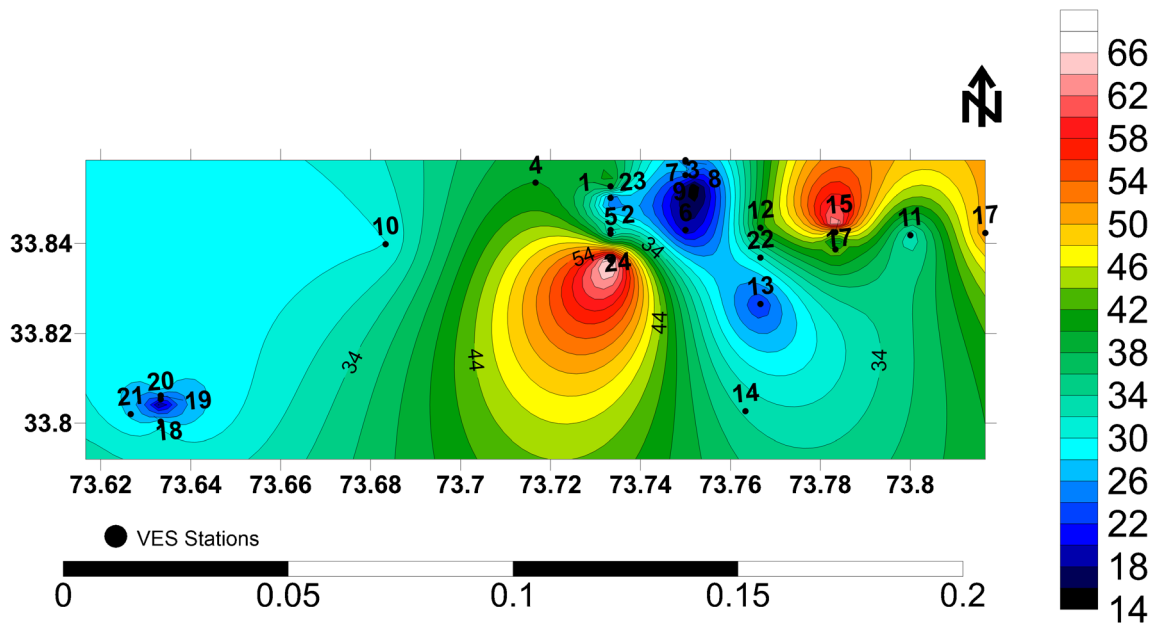


Fig. 3 2D iso-resistivity map at 15 m spacing

where T is transverse resistance and t is the total thickness of rock units

$\rho l = H/S$ where H is the total thickness and T is the longitudinal conductance

The parameter of anisotropy is the basic agents which controls the effective thickness and effective resistivity.

Anisotropic variations

The coefficient of anisotropy values (λ) lies between -0.4 and 4.2 (Fig. 9). The 3D maps displaying two peaks have figured out the highest anisotropy values above 3 at VES 10, 11, 17, 18, 19 and VES 20 in the northeastern and southwestern portion of study area. This relatively high values of coefficient of

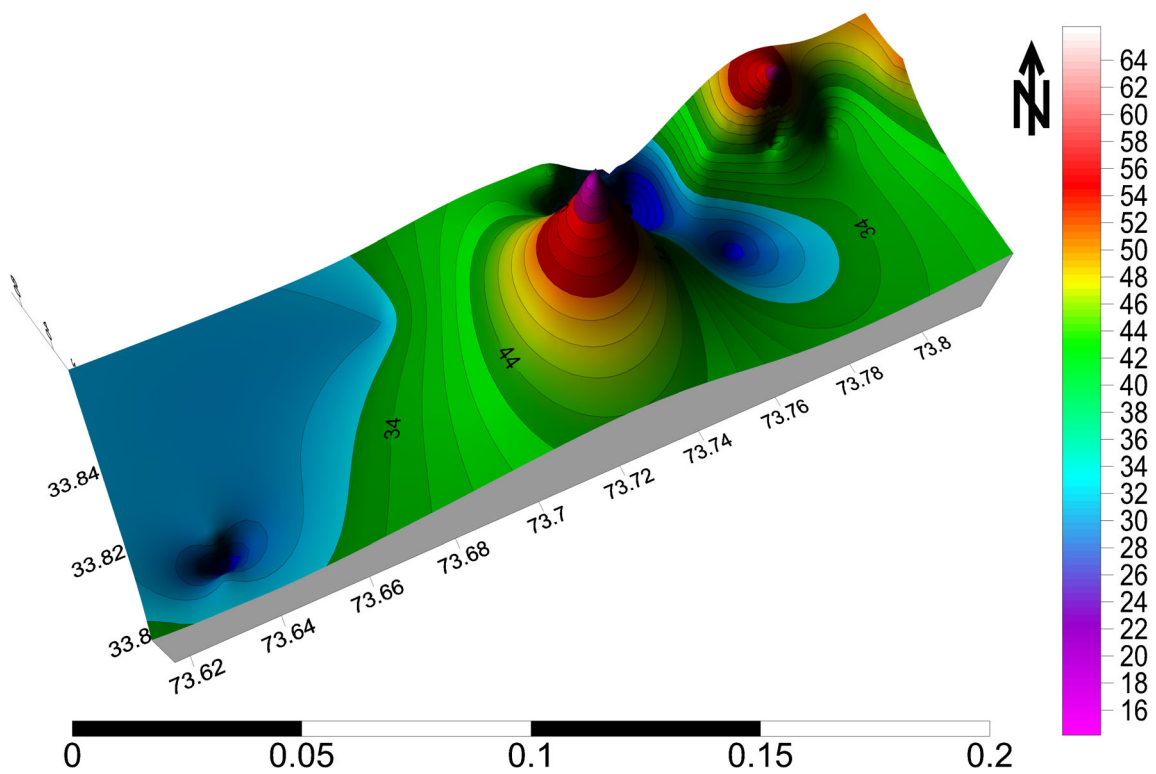


Fig. 4 3D iso-resistivity map at 15 m spacing

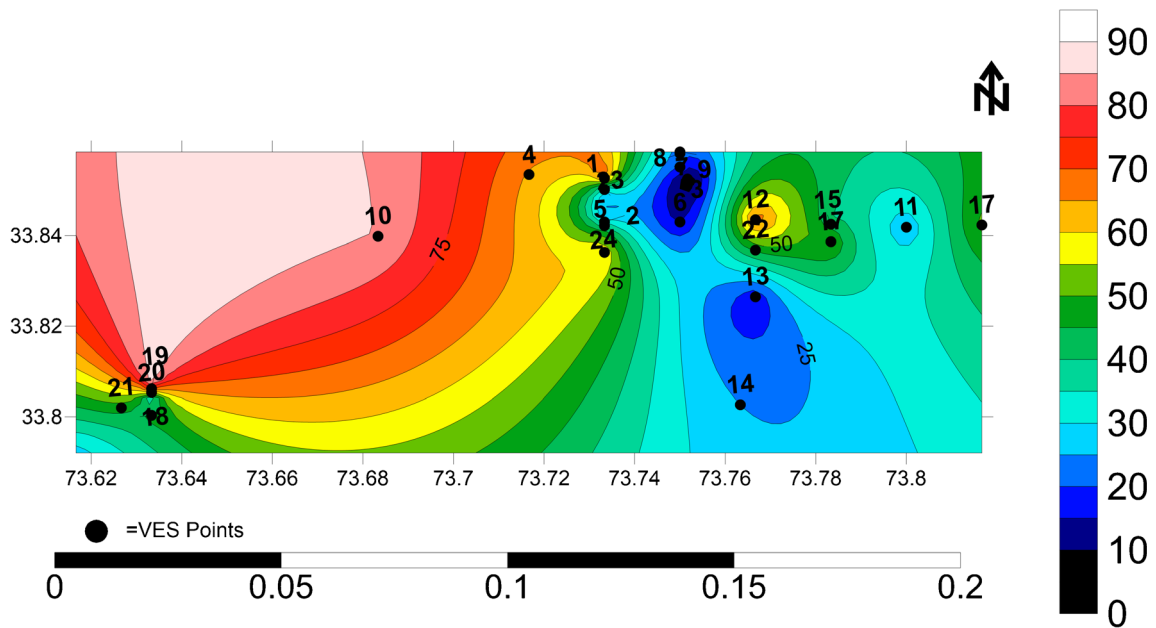


Fig. 5 2D isoresistivity map at 45 m spacing

anisotropy in northwestern and southeastern portion suggests that these are due to the near surface inhomogeneity and also due to the variation in structural features like faults, joints, and fractures and is relevant to the groundwater development in the area (Olasehinde and Bayewu 2011; Bayewu et al. 2014). The area is traversed by two faults (Fig. 1) Shaheed Gala Thrust and Riasi Thrust (Rustam et al. 2016). The high anisotropy values observed in this area are due to these faults. The other areas on map display lowest anisotropy values and hence show homogeneity and marked as alluvium.

Interpretation of VES curves

The VES curves in Fig. 10a, b were interpreted to find confined- and semi-confined-type aquifers in the area. The low resistivities in the third and fourth layers indicate the saturated sandstone bounded by shales (Fig. 9) form the confined aquifers. These low values of resistivity in VES 17, 11, 15 are due to presence of Fault Shaheed Gala Thrust, while in VES 10 and 23, low values are indicating good potential of groundwater due to another fault known as Riasi thrust. The

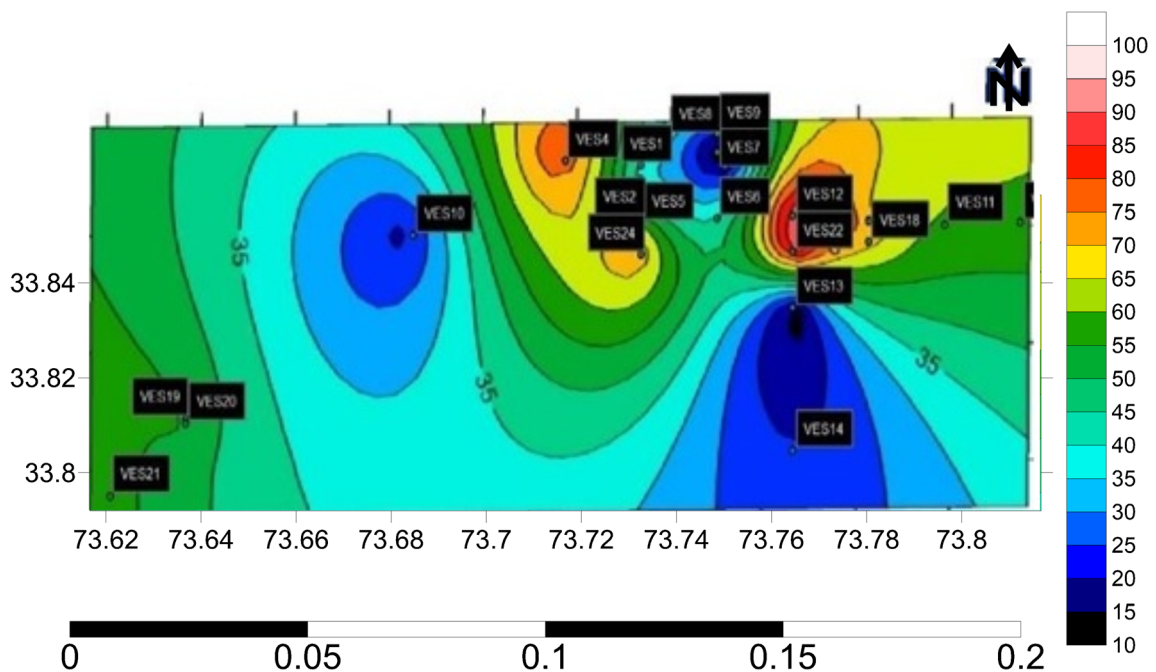


Fig. 6 2D isoresistivity map at 130 m spacing

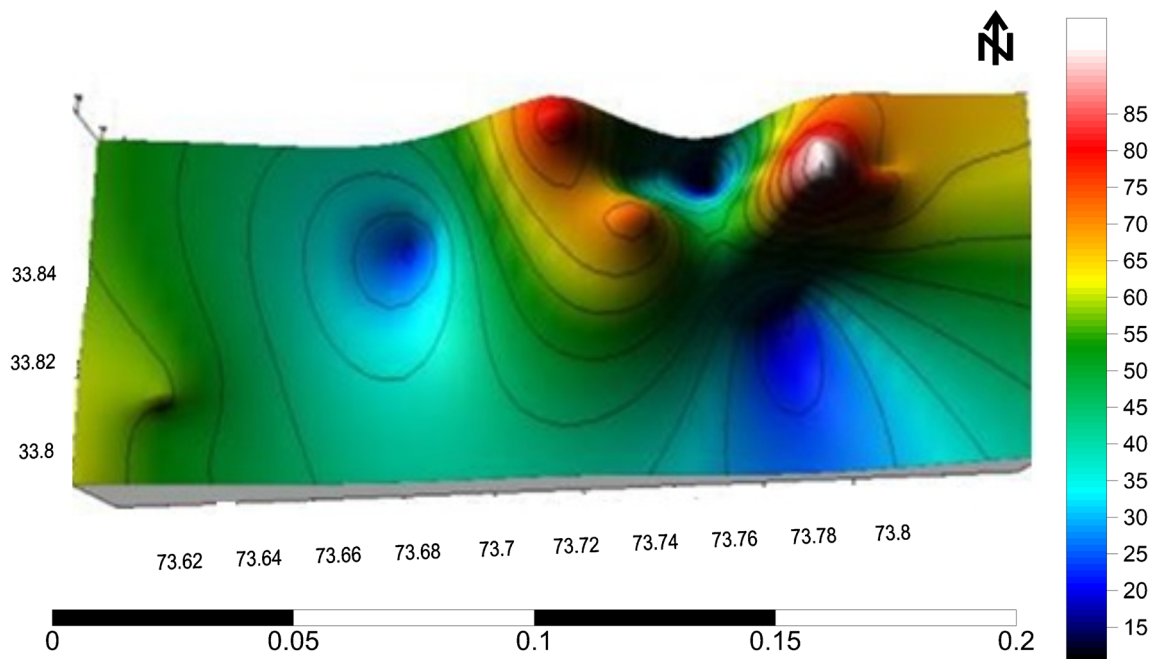


Fig. 7 3D isoresistivity map at 130 m spacing

faults are acting as a barrier for groundwater development (Niaz et al. 2016; Niaz et al. 2017). The interpretation reveals that area consist of confined and semi-confined aquifers with the considerable thickness. The tube wells can be installed in this area.

Petrography

The petrographic results indicate that the essential minerals such as quartz, feldspar, and rock fragments (igneous sedimentary and metamorphic origin) (Fig. 11) coexist in the rock.

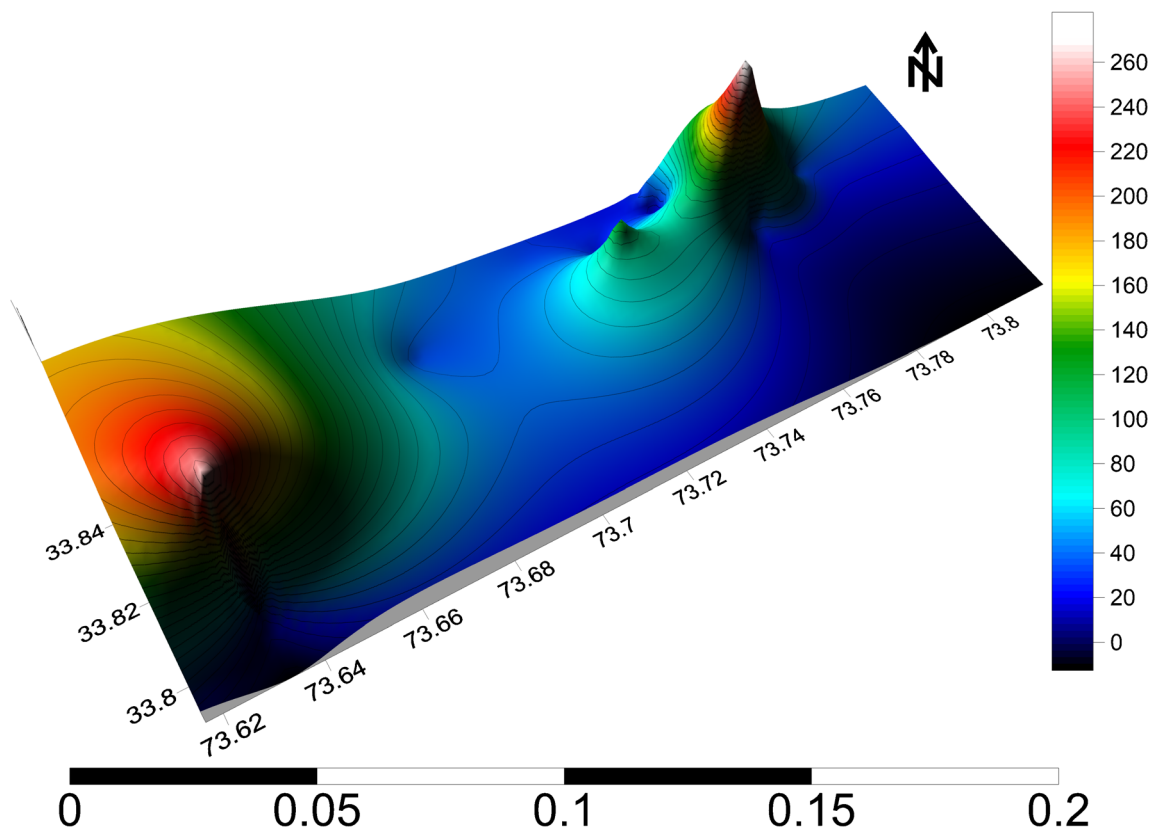


Fig. 8 3D isoresistivity map of transverse resistance

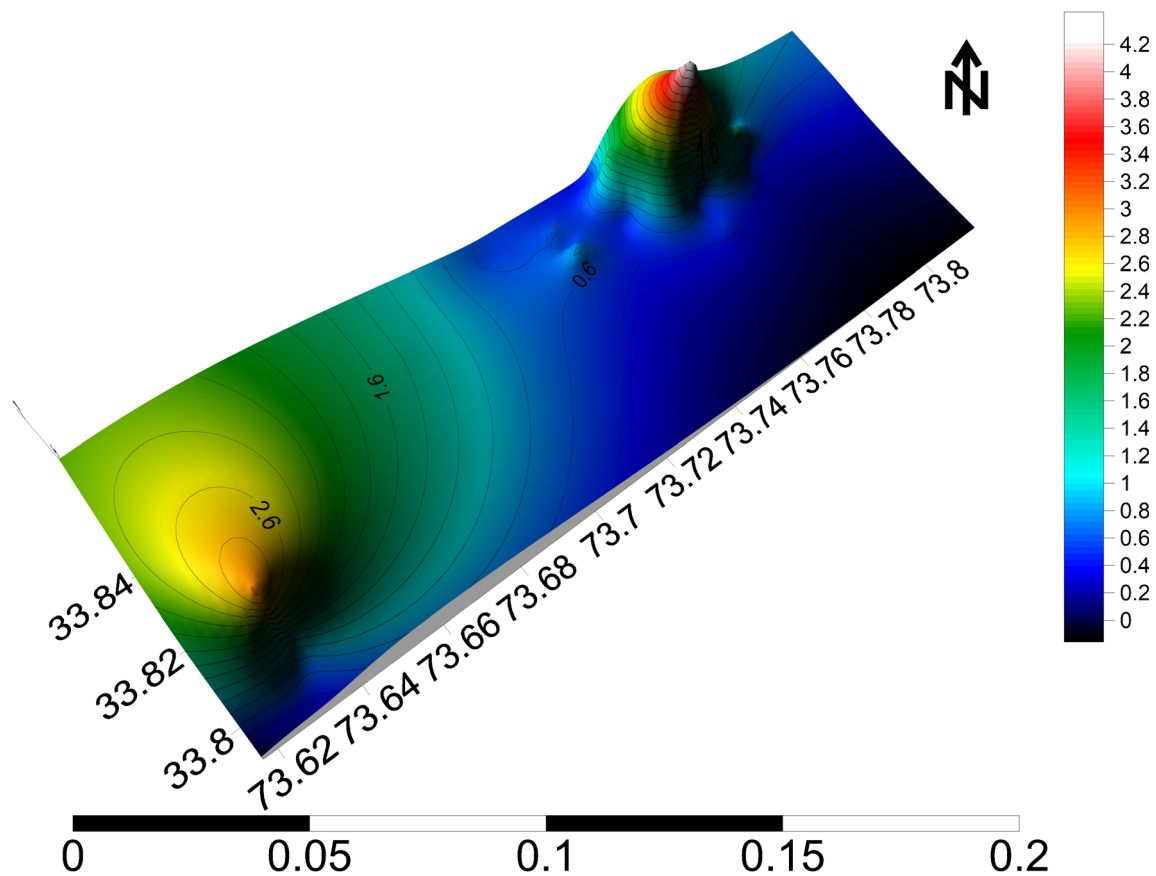


Fig. 9 3D isoresistivity map of anisotropy

The fracturing and chemical compaction of quartz (Fig. 11a, b, c, f), the decomposition of feldspar (Fig. 11d, e) and the ductile deformations of rock fragments (Fig. 11g) has developed secondary porosity (Bloch 1994) and affect the migration of fluids through the rocks. However, the pores formed by the dissolution are too small to develop effective porosity. The porosity in rock has been confirmed through the existence of fluids (Fig. 11h) during petrography.

Discussions

The rippled laminations and sheet-like sandstone interbedded with mudstone reveals crevasse splay deposits (Ulak 2009). The Laminated sandy mudstone and fine-grained sandstone are deposited by the floundering flow velocities of channel. The planar bedding (Fig. 2) has favored a sandy meandering and flood flow river system deposits (Ulak 2009). The planar stratified sandstone (Fig. 2) implies a shallower fluvial system and suggests upper flow regime origin for sandstone (Ulak 2009). The thick bedded mudstone and carbonate concretions in shale (Fig. 2) beds indicate a meandering stream pattern in a sinuous water

and flood flow. The calcareous concretions were originated under hydromorphic conditions in warm, arid to semiarid climates (Gile et al. 1965; Kraus 1999). The high bed and suspended loads have deposited the matrix-supported conglomerates (Harms et al. 1982). The mudstone was deposited in the flood-dominated alluvial fan environment (Searle et al. 1990; Blair and McPherson 1994).

The fluvial system of Siwaliks evolved through meandering to braided and finally formed flood plain system (Khan et al. 1997; Ulak and Nakayama 2001; Nakajima 1982; Hisatomi and Tanaka 1994; Zaleha 1997; Willis 1993). The upliftment of Himalayas towards the north is the main contributor of deposition in the Foreland basin (Ulak 2009). The flow direction as deduced through the ripple laminations and planar bedding (Fig. 2) indicates southward migration of channel.

The diversion of river pattern within the region has formed confined aquifers of the regions (Sapkota 2003). The aquifers confined between subsurface lithologies were interpreted by means of resistivity surveys. The medium and high-resistivity zones in the area were marked by vertical electrical sounding (VES) curves. The resistivity data is further interpreted to find the lithologies (boulders, sand, and clays overlying the area).

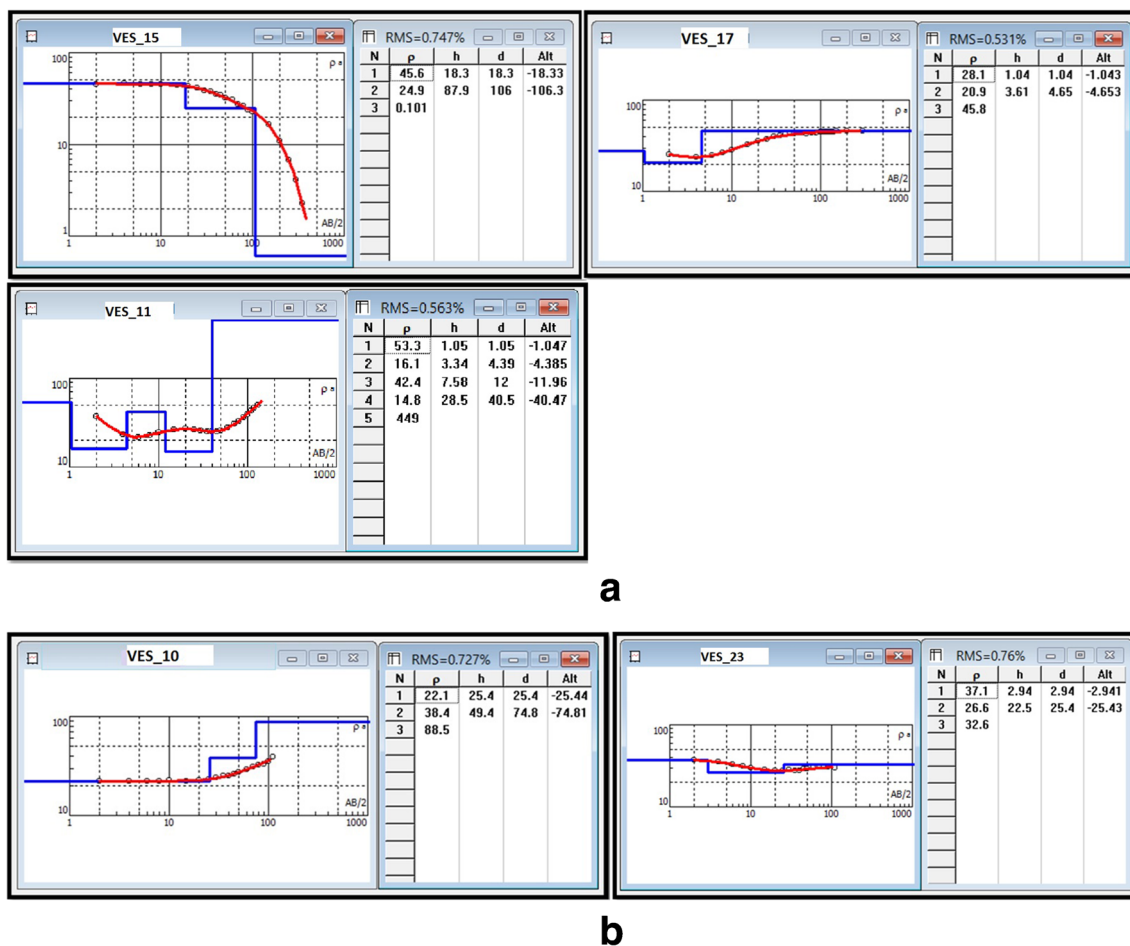


Fig. 10 **a** Interpreted of VES curve types. **b** Interpreted of VES curve types

The resistivity values are low in fine sediments and high in coarse sediments (Table 3). The sediments at shallow depth like those of near surface rocks are dominated by clays and sandy material as well as alluvium. The resistivity values in a few regions are also affected by the moisture content and fluids trapped in pore spaces of rocks (Fig. 11h). The fracturing, dissolution, and decomposition of minerals have developed secondary porosity in the rock to facilitate the movement of water through pores (Fig. 11).

Conclusion

The conjugate techniques, geoelectrical method, and petrographic analysis are very helpful for the identification of subsurface groundwater reserves. The lithofacies deposited by meandering, braided, and flood plain system during stream diversions in the area have formed aquifers of the region. There is strong correlation between the

exposed litho-log and the calculated thickness of lithologies on the bases of geoelectrical data. The qualitative and quantitative interpretations have revealed the presence of groundwater within formations and have figured out the confined and semi-confined-type aquifers in the sedimentary rocks. The apparent resistivity maps indicate the decrease in resistivity with the increase of depth pointing towards good groundwater potential in the area. The thick sandstone (10–42 m) at different locations indicates the promising groundwater potential in the area. The highest anisotropy values at the VES 10, 11, 17, 18, 19, 20, and 21 due to the regional faults in the area indicate the good groundwater potential. The petrography has provided the clues of the secondary porosity and

Fig. 11 The photomicrographs showing the deformations facilitating the secondary porosity in the rocks (a), b, c Fractures in quartz grains. d, e Feldspar decompositions. f Chemical compaction or pressure solution in quartz (as indicated by arrows on the confronting sides of light and dark band). g Ductile deformation of metamorphic rock fragment. h Porosity in sandstone

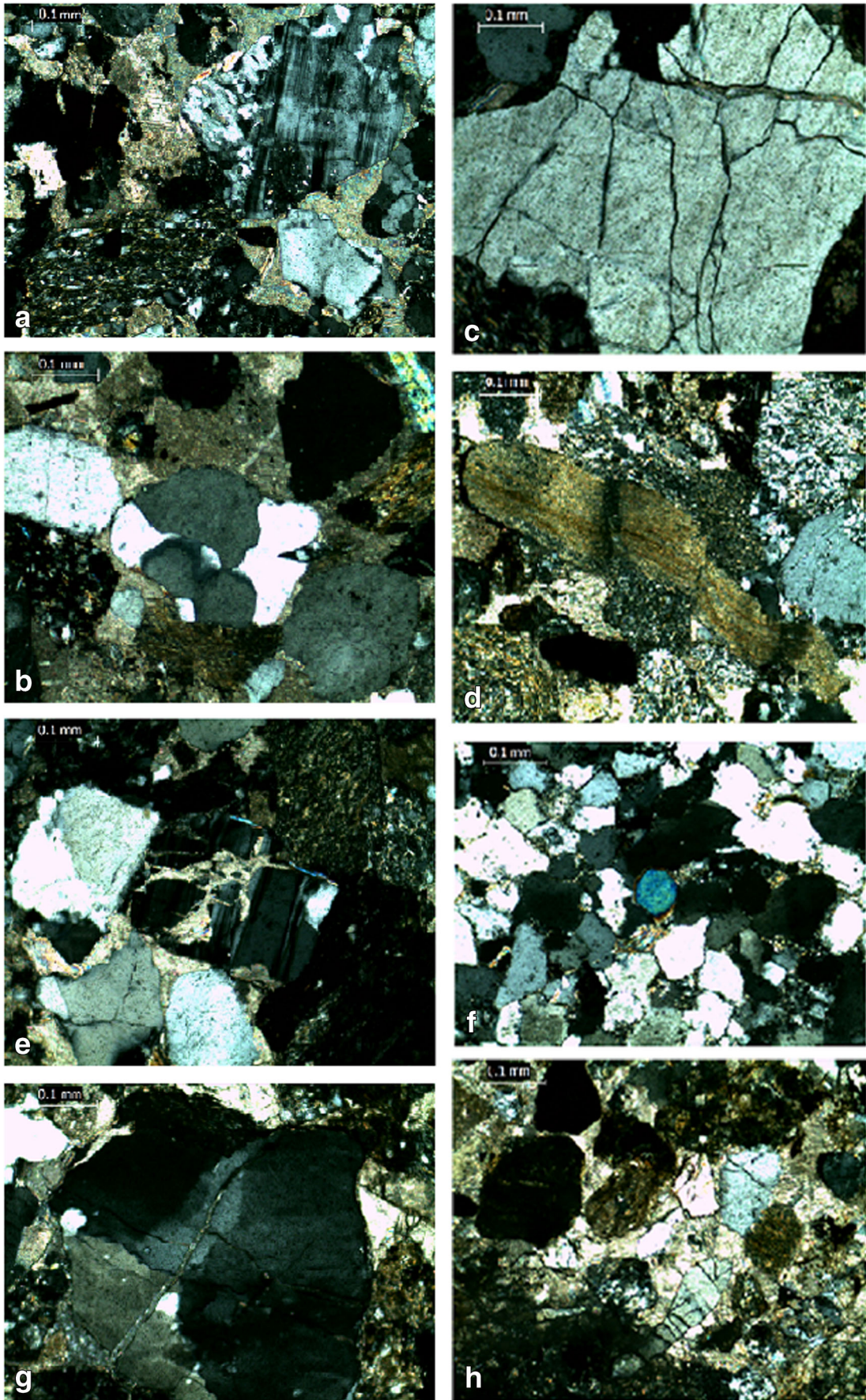


Table 3 The resistivity ranges of subsurface lithologies

Lithology	True resistivity (Ohm m)
Surface materials	39.8–40.9
Sandstone	123–3641
Boulder clays	0.841–84.9
Sandy clays	15.4–99.8
Siltstone	1.13–42.4
Clayey sand	49.3–58.2
Mudstone	20.9–61.7

fluid migrations through the rocks. So, the dug wells and tube wells can be installed in the area with promising endurance.

Funding information The Director Institute of Geology, University of Azad Jammu and Kashmir, Muzaffarabad provided the financial assistance to carry out the field work in the study area.

References

- Alile OM, Ujuanbi O, Evbuomwan IA (2011) Geoelectric investigation of groundwater in Obaretin -Iyanomon locality, Edo state, Nigeria. *J Geol Mining Res* 3(1):13–20
- Balaji S, Rahmam K, Jeganathan R, Neelakantan R (2010) Demarcation of fresh/saline water Interface in Kavaratti Island of union territory of Lakshadweep island of India using electrical and electromagnetic methods. *Int J Earth Sci Eng* 3:62–72
- Barseem M, El Tamamy A, Masoud M (2013) Hydrogeophysical evaluation of water occurrences in El Negila area, Northwestern coastal zone–Egypt. *J Appl Sci Res* 9:3244–3262
- Bayewu OO, Oloruntola MO, Mosuro G (2014) Evaluation of resistivity anisotropy of P^WEtrfdgvyb'abrts of Ijebu Igbo, southwestern, Nigeria using azimuthal resistivity survey (ARS) method. *J Geogr Geol* 6(4):140–152
- Blair TC, McPherson M (1994) Alluvial fans and their natural distinction from rivers based on morphology, hydraulic processes, sedimentary processes and facie assemblage. *J. Sediment Res A* 64:450–489
- Bloch S (1994) Secondary porosity in sandstones, significance, origin, relationship to subaerial unconformities, and effect on pre-drill reservoir quality prediction. *SEPM short course* 30:137–162
- Choudhury K, Saha DK, Chakraborty P (2001) Geophysical study for saline water intrusion in a coastal alluvial terrain. *J Appl Geophys* 46:189–200
- Compton R (1985) *Geology in the field*. John Wiley and Son, New York, p 398
- DeLima OAL, Clennell MB, Nery GG, Niwas S (2005) A volumetric approach for the resistivity response of freshwater shaly sandstones. *Geophysics* 70:1–10
- Dobrin MB (1988) *Introduction to geophysical prospecting*. McGraw-Hill, New York, p 867
- Elizondo GM, Lofthouse V (2010) Towards a sustainable use of water at home: understanding how much, where and why? *J Sustain Dev* 3(1):3–10
- Gile LH, Peterson FF, Grossman RB (1965) The K horizon—a master soil horizon of carbonate accumulation. *Soil Sci* 99:74–82
- Gowd SS (2004) Electrical resistivity survey to delineate the groundwater potential aquifers in Peddavanka watershed, Anantapur District, Andhra Pradesh. *Environ Geol* 46:118–131
- Harms JC, Southard JB, Walker RG, (1982) Structures and sequences in clastic rocks. *SEPM ShortCourse* 9.
- Hisatomi K, Tanaka S (1994) Climatic and environmental changes at 9 and 7.5 Ma in the Churia (Siwalik) group, west-Central Nepal. *Himal Geol* 15:161–180
- Hubbard SS, Rubin Y (2005) *Introduction to hydrogeophysics*. In *Hydrogeophysics* (pp. 3–21). Springer, Dordrecht
- Joseph OC (2012) Vertical electrical sounding (VES) methods to delineate potential groundwater aquifers in Akobo area, Ibadan, south-western Nigeria. *J Geol Min Res* 4:35–42
- Joshua EO, Odeyemi OO, Fawehinmi OO (2011) Geoelectric investigation of the groundwater potential of Moniya area, Ibadan. *J Geol Min Res* 3:54–62
- Khaled M, Galal G (2012) Study of groundwater occurrence and the impact of salt water intrusion in east bitter lakes area. Northwest Sinai, Egypt, by using the geophysical techniques. *Egypt Geophy Soc J* 10:1–12
- Khalil MH (2010) Hydro-geophysical configuration for the quaternary aquifer of Nuweiba alluvial fan. *J Environ Eng Geophys* 15:77–90
- Khan IA, Bridge JS, Kappelman J, Wilson R (1997) Evolution of Miocene fluvial environment, eastern Potwar plateau, northern Pakistan. *Sediment* 44(2):349–368
- Kraus MJ (1999) Paleosols in clastic sedimentary rocks: their geological applications. *Earth Sci Rev* 47:41–70
- Lutgens FK, Tarbuck EJ, Tasa D, (2014) *Essentials of geology*. Pearson Higher Ed
- Margat J, Van der Gun J (2013) *Groundwater around the world*. CRC Press/Balkema, Leiden
- Martinelli E (1978) Groundwater exploration by geoelectrical methods in southern Africa. *Bull Engin Geol* 15:113–124
- Maury S, Balaji S (2014) Geoelectrical method in the investigation of groundwater resource and related issues in ophiolite and flysch formations of Port Blair, Andaman Island, India. *Environ Earth Sci* 71: 183–199
- Nakajima T (1982) Sedimentology and uranium prospecting of the Siwaliks in western Nepal. *Bull Geol Surv Jpn* 33(12):593–617
- Niaz A, Khan MR, Mustafa S, Hameed F (2016) Determination of aquifer properties and vulnerability mapping by using geoelectrical investigation of parts of sub-Himalayas, Bhimber, Azad Jammu and Kashmir, Pakistan. *Q J Eng Geol Hydrogeol* 49:36–46
- Niaz A, Khan MR, Nisar UB, Khan S, Mustafa S, Hameed F, Mughal MS, Farooq M, Rizwan M (2017) The study of aquifers potential and contamination based on geoelectric technique and chemical analysis in Mirpur Azad Jammu and Kashmir, Pakistan. *J Himal Earth Sci* 50(2):60–73
- Niwas S, Gupta PK, de Lima OA (2006) Nonlinear electrical response of saturated shaley sand reservoir and its asymptotic approximations. *Geophysics* 71:G129–G133
- Nwanko C, Nwasu L, Emujakporue G (2011) Determination of Dar Zarouk parameters for assessment of groundwater potential: case study of Imo state, southeastern Nigeria. *J Econ Sustain Dev* 2:57–71
- Okafor P, Mamah L (2012) Integration of geophysical techniques for groundwater potential investigation in Katsina-ala, Benue state, Nigeria. *Pacific J Sci Technol* 13:463–474
- Olaschinde PI, Bayewu O (2011) Evaluation of electrical resistivity anisotropy in geological mapping: a case study of Odo Ara, west Central Nigeria. *Afr J Environ Sci Tech* 5:553–566
- Orellana E, Mooney H M, (1966) *Master Tables and Curves for Vertical Sounding Over Layered Structures*. Madrid: Interciencia
- Oseji J, Asokhia M, Okolie E (2006) Determination of groundwater potential in obiaruku and environs using surface geoelectric sounding. *Environmental* 26:301–308
- Ozcep F, Tezel O, Asci M (2009) Correlation between electrical resistivity and soil-water content: Istanbul and Golcuk. *Int J Phys Sci* 6(4): 362–365

- Parasnis DS (1979) Principles of applied geophysics, 3rd edn. Chapman & Hall, London
- Rustam MK, Hameed F, Mughal MS, Mustafa S (2016) Tectonic study of the sub-Himalayas based on geophysical data Azad Jammu and Kashmir and Northern Pakistan. *J Earth Sci* 27:981–988
- Sapkota B (2003) Hydrogeological conditions in the southern part of Dang valley, mid-western Nepal. *Him J. Sci* 1(2):119–122
- Searle MP, Pickering KT, Cooper DJW (1990) Restoration and evolution of intermontane Indus molasse basin, Ladakh Himalaya, India. *Tectonophysics* 174:301–314
- Siebert S, Burke J, Faures JM, Frenken K, Hoogeveen J, Döll P, Portmann FT (2010) Groundwater use for irrigation—a global inventory. *Hydrol Earth Syst Sci* 14:1863–1880
- Sikandar P, Bakhsh A, Arshad M, Rana T (2010) The use of vertical electrical sounding resistivity method for the location of low salinity groundwater for irrigation in Chaj and Rachna doabs. *Environ Earth Sci* 60:1113–1129
- Smith M, Cross K, Paden M, Laban P (2016) Spring—managing groundwater sustainably. IUCN, Gland, pp 17–20
- Thakur V, Jayangondaperumal R, Malik M (2010) Redefining Medlicott–Wadia’s main boundary fault from Jhelum to Yamuna: an active fault strand of the main boundary thrust in northwest Himalaya. *Tectonophysics* 489:29–42
- Ulak PD (2009) Lithostratigraphy and late Cenozoic fluvial styles of Siwalik group along Kankai River section, East Nepal Himalaya. *Bull Dep Geol, Tribhuvan University, Kathmandu, Nepal* 12:63–74
- Ulak PD, Nakayama K (2001) Neogene fluvial systems in the Siwalik group along the Tinau Khola section, west-Central Nepal Himalaya. *J Nepal Geol Soc* 25:111–122
- Willis B (1993) Evolution of Miocene fluvial systems in the Himalayan foredeep through a two kilometer-thick succession in northern Pakistan. *Sediment Geol* 88:77–121
- Yungul SH (1996) Electrical methods in geophysical exploration of sedimentary basins. Chapman & Hill, London
- Zaleha MJ (1997) Fluvial and lacustrine paleoenvironments of the Miocene Siwalik group, Khur area, northern Pakistan. *Sedimentol* 44(2):221–252